

Synthesis and Structural Characterization of $\text{Na}_x\text{Si}_{136}$ ($0 < x \leq 24$) Single Crystals and Low-Temperature Transport of Polycrystalline Specimens

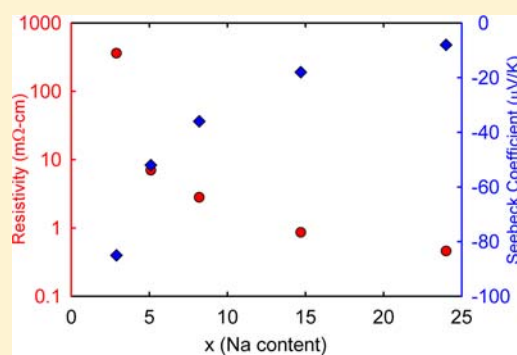
Stevce Stefanoski,[†] Christos D. Malliakas,[‡] Mercouri G. Kanatzidis,[‡] and George S. Nolas^{*,†}

[†]Department of Physics, University of South Florida, Tampa, Florida 33620, United States

[‡]Department of Chemistry, Northwestern University, Evanston, Illinois 60208, United States

Supporting Information

ABSTRACT: $\text{Na}_x\text{Si}_{136}$ clathrate-II single crystals with $x = 2.9, 5.1, 8.2,$ and 14.7 were prepared by a two-step process. In the first step, $\text{Na}_{24}\text{Si}_{136}$ single crystals were grown from the precursor Na_4Si_4 by reaction of the vapor phase with spatially separated graphite in a closed volume. In the second step, the $\text{Na}_{24}\text{Si}_{136}$ single crystals were subjected to thermal decomposition in a nitrogen atmosphere at 10 Torr and 405 °C. The Na content was controlled by the duration of thermal decomposition. The structural properties were investigated using single-crystal X-ray diffraction and compared with those of single-crystal $\text{Na}_{24}\text{Si}_{136}$. The quality of the obtained products also allowed for low-temperature transport property measurements on agglomerates of crystals allowing for an investigation into the low-temperature electrical and thermal properties as a function of Na content.



1. INTRODUCTION

The interest in group 14 clathrates stems from the unique properties that have been reported in these materials,^{1–4} including a very low thermal conductivity,^{1,5,6} magnetism,^{7,8} and superconductivity.^{9,10} These properties are a consequence of the structure and bonding of these materials.^{11–20} They are of both scientific and technological interest. Of the structure types that comprise the different clathrate phases, clathrate-II compositions have been among the least studied, although these materials have revealed interesting structural and physical properties since the early work of Cros and co-workers.^{21–23} This is partially because phase-pure preparation of these materials has been challenging. Nevertheless, a fundamental understanding of the structure–property relationships in these materials is important in assessing their potential for technologically useful applications.^{1–5,8,9,13,14,16,18,24–26} To this end, improved synthetic techniques have been developed in continuing and expanding the investigation into these materials.^{11–13,15,27–34} Of these techniques, the preparation of single crystals allowed for intrinsic property measurements.^{27,30,34–37} For example, the synthesis of single-crystal $\text{Na}_{24}\text{Si}_{136}$ by spark-plasma sintering³⁰ and single-crystal $\text{Na}_8\text{Si}_{46}$ synthesized by vapor-phase intercalation of Na with graphite²⁷ allowed for improved physical property measurements compared with that of our previous results.^{29,34,36,38}

The clathrate-II crystal structure can be represented by the general formula $\text{X}_8\text{Y}_{16}\text{E}_{136}$ (space group $Fd\bar{3}m$) where E represents group 14 elements forming completely or partially filled “polyhedral cages” and X and Y represent atoms that are located inside hexakaidecahedra (Si_{28}) and dodecahedra (Si_{20}),

respectively.^{1,14,39} Framework doping, or substitution, is also possible.^{40,41} The synthesis and characterization of microcrystalline powders of partially filled $\text{Na}_x\text{Si}_{136}$ clathrate-II compositions with less than full Na occupancy revealed structural properties that are fundamental to this material system.^{11,12,28} Herein we report on the synthesis and structural properties of single crystals of $\text{Na}_x\text{Si}_{136}$. Our two-step synthetic approach also allowed for low-temperature transport measurements of polycrystalline $\text{Na}_x\text{Si}_{136}$. Together with our previous results on single-crystal $\text{Na}_{24}\text{Si}_{136}$,²⁷ we investigate the structural, electrical, and thermal properties of $\text{Na}_x\text{Si}_{136}$ with $x = 2.9, 5.1, 8.2, 14.7,$ and 24 .

2. EXPERIMENTAL SECTION

The Na_4Si_4 precursor was synthesized by direct reaction of elemental Na (Alfa Aesar, 99.98%) and Si powder (Alfa Aesar, 99%). A Na/Si atomic ratio of 1.1:1 was placed inside a tungsten crucible that was inside a sealed stainless steel canister and reacted at 650 °C for 36 h. The resulting product was a dark gray crystalline material. The product was ground into coarse powder in a dry nitrogen atmosphere and used as the precursor for $\text{Na}_{24}\text{Si}_{136}$ single-crystal growth. This was achieved via the slow controlled removal of Na from the Na_4Si_4 precursor by vapor phase intercalation with spatially separated graphite. The details of this technique were reported previously.²⁷ $\text{Na}_{24}\text{Si}_{136}$ single-crystals obtained in this way were enclosed in tantalum envelopes which were sealed inside a 10 in. long quartz tube with a 15 mm diameter in a nitrogen atmosphere and placed in a tube furnace. A thermal gradient was established along the tube, where the hot end was held at 405 °C and the cold end at approximately 390 °C. This allowed for Na to

Received: October 11, 2011

Published: August 8, 2012

Table 1. Crystallographic and Structure Refinement Data for $\text{Na}_x\text{Si}_{136}$ ^a

| property | composition | | | | |
|---|----------------------------------|----------------------------------|----------------------------------|-----------------------------------|---------------------------------|
| | $\text{Na}_{2.9}\text{Si}_{136}$ | $\text{Na}_{5.1}\text{Si}_{136}$ | $\text{Na}_{8.2}\text{Si}_{136}$ | $\text{Na}_{14.7}\text{Si}_{136}$ | $\text{Na}_{24}\text{Si}_{136}$ |
| x (Si_{20}) | 0 | 0 | 1.5 | 6.7 | 16 |
| x (Si_{28}) | 2.9 | 5.1 | 6.7 | 8 | 8 |
| lattice param | 14.6522(17) | 14.6437(7) | 14.6423(7) | 14.6500(7) | 14.7121(1) |
| density | 2.052 | 2.082 | 2.120 | 2.196 | 2.280 |
| abs coeff, μ | 1.351 | 1.361 | 1.373 | 1.395 | 1.411 |
| GOF on F^2 | 1.513 | 1.496 | 1.442 | 1.399 | 1.000 |
| $R_1, I > 2\sigma(I)$ | 0.0393 | 0.0288 | 0.0283 | 0.0312 | 0.0115 |
| wR_2 , all data | 0.0574 | 0.0528 | 0.0584 | 0.0628 | 0.0290 |
| largest diff. peak ($e/\text{\AA}^3$) | 0.441 | 0.589 | 0.305 | 0.497 | 0.203 |
| largest diff. hole ($e/\text{\AA}^3$) | -0.401 | -0.266 | -0.308 | -0.518 | -0.122 |

^aLattice parameters are given in \AA , densities in g/cm^3 , and absorption coefficients in mm^{-1} .

leave the $\text{Na}_{24}\text{Si}_{136}$ clathrate crystals, or “degas”, and condense on the cold end. Scanning electron microscope (SEM) analyses using a JEOL JSM-6390LV indicated that the resulting products were polycrystalline specimens comprised of several densely packed large grains. $\text{Na}_x\text{Si}_{136}$ single crystals were separated from the polycrystalline specimens and used for single-crystal X-ray diffraction analyses (after low-temperature transport measurements were conducted, as will be described below). X-ray data for the $\text{Na}_x\text{Si}_{136}$ single crystals were obtained at 200 K on a STOE diffractometer using a graphite monochromator and a Mo $K\alpha$ fine-focus sealed tube with a wavelength of 0.71073 \AA . $\text{Na}_x\text{Si}_{136}$ compositions with $x = 2.9, 5.1, 8.2,$ and 14.7 were obtained after placing the $\text{Na}_{24}\text{Si}_{136}$ crystals in a tube furnace at 405 $^\circ\text{C}$ for 24, 12, 4, and 2 days, respectively. Refining the crystal structure using SHELXL-97 for a few different single crystals separated from the same agglomerate of crystals indicated only a small variation in x and full occupancy of the Si framework for all crystals. Table 1 contains the crystallographic and single-crystal structure refinement information for $\text{Na}_x\text{Si}_{136}$. Atomic coordinates and atomic displacement parameters for the $\text{Na}_x\text{Si}_{136}$ compositions are given in Table 2. The Na–Si and Si–Si interatomic distances obtained from the single-crystal refinement are listed in Table 3, and selected Si–bond angles are given in Table 4.

Powder X-ray diffraction (pXRD) patterns obtained from crushed crystals, shown in Figure 1, were collected with a Bruker D8 Focus

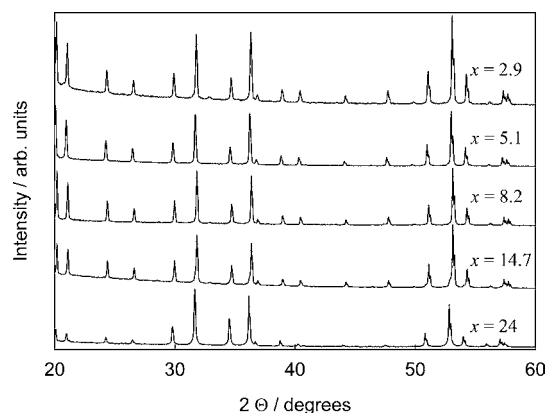


Figure 1. pXRD data obtained from crushed $\text{Na}_x\text{Si}_{136}$ crystals.

diffractometer in Bragg–Brentano geometry using Cu $K\alpha$ radiation and a graphite monochromator. The relative intensities of the peaks in Figure 1 are similar to those obtained from simulated patterns using the crystallographic data in Table 2.

The Seebeck coefficient, S , four-probe resistivity, ρ , and steady-state thermal conductivity, κ , were measured on the agglomeration of crystals using a custom radiation-shielded vacuum probe.⁴² Due to the small size of these polycrystalline specimens (less than 1 mm), Cu wires (0.076 mm in diameter) were attached to the surface of the

specimen using silver epoxy. At the opposite ends of these Cu wires, voltage probes were attached using silver epoxy and thermocouple contacts using stycast, in order to measure the potential difference across the same two points at which the temperature difference was measured. Electrical current was sourced using Cu wires (0.025 mm in diameter) attached to the opposite ends of the specimen. Conservative estimates of the room-temperature maximum uncertainties in the measurement of S , ρ , and κ are 6%, 30%, and 30%, respectively. The relatively large maximum uncertainties estimated for ρ and κ are due to the relatively large contacts compared with the size of the specimens.

3. RESULTS AND DISCUSSION

As shown in Figure 2, the Si_{136} framework in clathrate-II $\text{Na}_x\text{Si}_{136}$ is built of covalently bonded Si atoms forming two

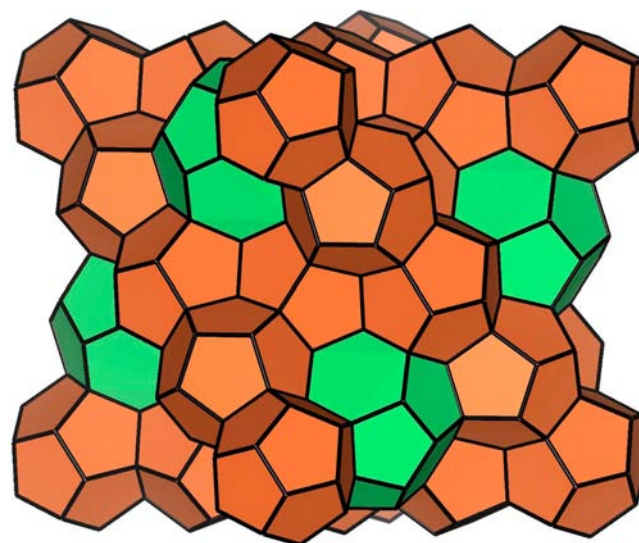


Figure 2. Crystal structure of $\text{Na}_x\text{Si}_{136}$ with Si_{20} shown in orange and Si_{28} in green.

types of polyhedra: Si_{20} dodecahedra, centered at 16c crystallographic sites (000) with $\bar{3}m$ symmetry, and Si_{28} hexakaidecahedra, centered at $8b$ crystallographic sites ($3/8, 3/8, 3/8$) with $4\bar{3}m$ symmetry.^{1,14,39} There are 16 Si_{20} and 8 Si_{28} per conventional unit cell in clathrate-II $\text{Na}_x\text{Si}_{136}$, the occupancy of which can vary.^{11,12,28,29,43}

The lattice parameters of $\text{Na}_x\text{Si}_{136}$, given in Table 1, exhibit a nonmonotonic behavior. They decrease with increasing x up to $x = 8$ and then increase with increasing x from $x = 8$ to 24. This initial lattice contraction at low Na concentration was

Table 2. Atomic Coordinates and Atomic Displacement Parameters (Å) in Na_xSi₁₃₆^a

| atom | x | y | z | U ₁₁ | U ₂₂ | U ₃₃ | U ₂₃ | U ₁₃ | U ₁₂ | U _{eq} |
|--------------------------------------|------------|------------|------------|-----------------|-----------------|-----------------|-----------------|-----------------|-----------------|-----------------|
| Na _{2,9} Si ₁₃₆ | | | | | | | | | | |
| Na2 | 0.1250 | 0.6250 | 0.0949(15) | 0.034(8) | 0.034(8) | 0.006(9) | 0 | 0 | -0.003(6) | 0.025(8) |
| Si1 | 0.1250 | 0.1250 | 0.1250 | 0.0040(3) | 0.0040(3) | 0.0040(3) | 0 | 0 | 0 | 0.0040(3) |
| Si2 | 0.03288(4) | 0.21712(4) | 0.03288(4) | 0.00391(17) | 0.00391(17) | 0.00391(17) | 0.00025(17) | -0.00025(17) | 0.00025(17) | 0.00391(17) |
| Si3 | 0.06744(3) | 0.37055(4) | 0.06744(3) | 0.00382(15) | 0.0041(2) | 0.00382(15) | 0.00006(12) | 0.00063(15) | 0.00006(12) | 0.00390(12) |
| Na _{5,1} Si ₁₃₆ | | | | | | | | | | |
| Na2 | 0.1250 | 0.6250 | 0.0994(14) | 0.051(10) | 0.051(10) | 0.020(8) | 0 | 0 | -0.008(6) | 0.041(8) |
| Si1 | 0.1250 | 0.1250 | 0.1250 | 0.0041(3) | 0.0041(3) | 0.0041(3) | 0 | 0 | 0 | 0.0041(3) |
| Si2 | 0.03285(3) | 0.21715(3) | 0.03285(3) | 0.00400(15) | 0.00400(15) | 0.00400(15) | 0.00021(14) | -0.00021(14) | 0.00021(14) | 0.00400(15) |
| Si3 | 0.06738(2) | 0.37064(3) | 0.06738(2) | 0.00386(13) | 0.00416(19) | 0.00386(13) | 0.00010(10) | 0.00054(13) | 0.00010(10) | 0.00396(11) |
| Na _{8,2} Si ₁₃₆ | | | | | | | | | | |
| Na1 | 0.0000 | 0.0000 | 0.0000 | 0.003(3) | 0.003(3) | 0.003(3) | -0.001(2) | -0.001(2) | -0.001(2) | 0.003(3) |
| Na2 | 0.1250 | 0.6250 | 0.1007(13) | 0.052(6) | 0.052(6) | 0.046(8) | 0 | 0 | -0.002(4) | 0.050(7) |
| Si1 | 0.1250 | 0.1250 | 0.1250 | 0.0039(3) | 0.0039(3) | 0.0039(3) | 0 | 0 | 0 | 0.0039(3) |
| Si2 | 0.03271(3) | 0.21729(3) | 0.03271(3) | 0.00379(15) | 0.00379(15) | 0.00379(15) | 0.00007(14) | -0.00007(14) | 0.00007(14) | 0.00379(15) |
| Si3 | 0.06734(2) | 0.37072(3) | 0.06734(2) | 0.00361(14) | 0.0040(2) | 0.00361(14) | 0.00010(10) | 0.00055(13) | 0.00010(10) | 0.00374(12) |
| Na _{14,7} Si ₁₃₆ | | | | | | | | | | |
| Na1 | 0.0000 | 0.0000 | 0.0000 | 0.0130(16) | 0.0130(16) | 0.0130(16) | -0.0017(12) | -0.0017(12) | -0.0017(12) | 0.0130(16) |
| Na2 | 0.1250 | 0.6250 | 0.1014(19) | 0.056(10) | 0.056(10) | 0.037(10) | 0 | 0 | -0.001(6) | 0.050(8) |
| Si1 | 0.1250 | 0.1250 | 0.1250 | 0.0047(3) | 0.0047(3) | 0.0047(3) | 0 | 0 | 0 | 0.0047(3) |
| Si2 | 0.03240(4) | 0.21760(4) | 0.03240(4) | 0.00445(18) | 0.00445(18) | 0.00445(18) | 0.00021(17) | -0.00021(17) | 0.00021(17) | 0.00445(18) |
| Si3 | 0.06727(3) | 0.37098(4) | 0.06727(3) | 0.00420(17) | 0.0049(2) | 0.00420(17) | 0.00015(12) | 0.00048(16) | 0.00015(12) | 0.00443(14) |
| Na _{2,3} Si ₁₃₆ | | | | | | | | | | |
| Na1 | 0.0000 | 0.0000 | 0.0000 | 0.013(2) | 0.013(2) | 0.013(2) | -0.001(1) | -0.001(1) | -0.001(1) | 0.0152(2) |
| Na2 | 0.1250 | 0.6250 | 0.1466(7) | 0.057(10) | 0.057(10) | 0.037(10) | -0.001(3) | 0 | 0 | 0.049(3) |
| Si1 | 0.1250 | 0.1250 | 0.1250 | 0.006(1) | 0.006(1) | 0.006(1) | 0 | 0 | 0 | 0.00613(18) |
| Si2 | 0.0320(1) | 0.2180(1) | 0.0320(1) | 0.006(1) | 0.006(1) | 0.006(1) | 0.000(1) | 0.000(1) | 0.000(1) | 0.00636(10) |
| Si3 | 0.0674(1) | 0.3713(1) | 0.0674(1) | 0.006(1) | 0.006(1) | 0.006(1) | 0.000(1) | 0.000(1) | 0.000(1) | 0.00649(8) |

^aAtomic positions in Wyckoff notation: Na1 (16c), Na2 (48f), Si1 (8a), Si2 (32e), Si3 (96g).

Table 3. Na–Si and Si–Si Atomic Distances (Å) for $\text{Na}_x\text{Si}_{136}$

| | composition | | | | |
|--------------|----------------------------------|----------------------------------|----------------------------------|-----------------------------------|---------------------------------|
| | $\text{Na}_{2.9}\text{Si}_{136}$ | $\text{Na}_{5.1}\text{Si}_{136}$ | $\text{Na}_{8.2}\text{Si}_{136}$ | $\text{Na}_{14.7}\text{Si}_{136}$ | $\text{Na}_{24}\text{Si}_{136}$ |
| Na1–Si1 | <i>a</i> | <i>a</i> | 3.17015(15) × 2 | 3.17182(15) × 2 | 3.1853(2) × 2 |
| Na1–Si2 | <i>a</i> | <i>a</i> | 3.2529(4) × 6 | 3.2578(4) × 6 | 3.2753(2) × 6 |
| Na1–Si3 | <i>a</i> | <i>a</i> | 3.3541(3) × 12 | 3.3584(4) × 12 | 3.3740(2) × 12 |
| Na2–Si2 | 3.769(11) × 2 | 3.799(10) × 2 | 3.788(13) × 2 | 3.805(14) × 2 | 3.828(10) × 2 |
| Na2–Si2 | 4.277(14) × 2 | 4.232(13) × 2 | 4.206(16) × 2 | 4.203(17) × 2 | 4.192(12) × 2 |
| Na2–Si3 | 3.50(2) × 2 | 3.555(19) × 2 | 3.56(2) × 2 | 3.58(3) × 2 | 3.622(18) × 2 |
| Na2–Si3 | 3.769(11) × 4 | 3.728(13) × 4 | 3.709(17) × 4 | 3.747(18) × 4 | 3.787(12) × 4 |
| Na2–Si3 | 3.844(2) × 4 | 3.848(2) × 4 | 3.850(3) × 4 | 3.849(4) × 4 | 3.865(3) × 4 |
| Na2–Si3 | 4.005(2) × 2 | 3.9961(16) × 2 | 3.9920(19) × 2 | 3.998(8) × 2 | 4.0112(13) × 2 |
| Na2–Si3 | 4.020(3) × 2 | 4.008(2) × 2 | 3.997(8) × 2 | 4.004(3) × 2 | 4.001(5) × 2 |
| Na2–Si3 | 4.033(7) × 2 | 4.009(6) × 2 | 4.003(3) × 2 | 4.203(17) × 2 | 4.0199(18) × 2 |
| Na2–Si3 | 4.277(14) × 2 | 4.232(15) × 2 | 4.231(19) × 2 | 4.24(2) × 2 | 4.232(14) × 2 |
| Na2–Si3 | 4.34 (2) × 2 | 4.270(19) × 2 | 4.24(2) × 2 | 4.24(3) × 2 | 4.222(18) × 2 |
| Si1–Si2 | 2.3378(10) × 4 | 2.3372(8) × 4 | 2.3405(8) × 4 | 2.3498(10) × 4 | 2.3691(5) × 4 |
| Si2–Si1 | 2.3377(10) | 2.3372(8) | 2.3406(8) | 2.3498(10) | 2.3691(5) |
| Si2–Si3 | 2.3594(7) × 4 | 2.3587(5) × 4 | 2.3582(5) × 4 | 2.3602(7) × 4 | 2.3726(3) × 4 |
| Si3–Si3 | 2.3574(6) × 2 | 2.3540(5) × 2 | 2.3524(5) × 2 | 2.3498(6) × 2 | 2.3581(3) × 2 |
| Si3–Si3 | 2.3853(11) × 2 | 2.3867(9) × 2 | 2.3880(9) × 2 | 2.3922(11) × 2 | 2.3975(6) × 2 |
| Na1–Si (avg) | <i>a</i> | <i>a</i> | 3.3053 | 3.3096 | 3.3255 |
| Na2–Si (avg) | 3.9539 | 3.9378 | 3.9279 | 3.9554 | 3.9527 |
| Si–Si (avg) | 2.3548 | 2.3540 | 2.3551 | 2.3595 | 2.3729 |

^aNot applicable.

Table 4. Selected Angles (deg) for $\text{Na}_x\text{Si}_{136}$

| angle | composition | | | | |
|-------------|----------------------------------|----------------------------------|----------------------------------|-----------------------------------|---------------------------------|
| | $\text{Na}_{2.9}\text{Si}_{136}$ | $\text{Na}_{5.1}\text{Si}_{136}$ | $\text{Na}_{8.2}\text{Si}_{136}$ | $\text{Na}_{14.7}\text{Si}_{136}$ | $\text{Na}_{24}\text{Si}_{136}$ |
| Si2–Si1–Si2 | 109.5 | 109.5 | 109.5 | 109.5 | 109.5 |
| Si1–Si2–Si3 | 107.60(3) | 107.62(2) | 107.56(2) | 107.44(3) | 107.201(5) |
| Si3–Si2–Si3 | 111.28(2) | 111.26(2) | 111.31(2) | 111.42(2) | 111.643(13) |
| Si3–Si3–Si2 | 105.67(3) | 105.69(2) | 105.66(2) | 105.56(3) | 105.277(17) |
| Si3–Si3–Si3 | 108.68(2) | 108.669(19) | 108.671(19) | 108.72(2) | 108.898(13) |
| Si3–Si3–Si3 | 119.851(4) | 119.849(3) | 119.850(3) | 119.846(4) | 119.813(2) |

previously predicted by density functional theory (DFT)²⁶ and was later observed from pXRD on microcrystalline $\text{Na}_x\text{Si}_{136}$ powders.²⁸ From the relative occupancies of the two different polyhedra, Na vacates Si_{20} first. After Si_{20} are empty, Na vacates Si_{28} . This preferential occupation of Si_{28} has also been observed in gas hydrates with the clathrate-II structure.⁴⁴ Because of the different size and coordination number for Si_{20} and Si_{28} , a difference in the structural properties can be anticipated with different Na content.

Atomic coordinates, isotropic atomic displacement parameters, U_{eq} , and anisotropic atomic displacement parameters, U_{ij} , are given in Table 2. The results are consistent with those of pXRD.²⁸ All Si framework sites were found to be fully occupied, whereas the occupancy of the Na “guest” sites varies between $x = 2.9$ and 24. Na1 at the 16c crystallographic site was best refined at the center of Si_{20} . Because of the very large atomic displacement parameters for Na2 at the 8b crystallographic site in Si_{28} , a split-site model was used with Na “off-center” (the 48f crystallographic site, Table 2). The R_1 and wR_2 indices were slightly higher when Na was refined “off-center” compared with when refined at the 8b crystallographic site; however, this resulted in lower atomic displacement parameters. This is in agreement with previous studies on $\text{Na}_x\text{Si}_{136}$ ^{14,26–28,36,37,45–47} and suggests that Na2 displaces off-center along the z-direction, in contrast to the case of $\text{K}_{17.8}\text{Si}_{136}$, where K inside Si_{28} was best

refined at the center of Si_{28} .⁴⁸ U_{eq} for Na2 have similar values for $x \geq 8$, then decrease with decreasing x . This may be an indication that the nearest-neighbor Si_{28} sites vacate last, since interactions between Na are negligible for distances larger than the shortest Na–Na distance.⁴⁹ U_{eq} for Na1 decrease with decreasing x , as does U_{eq} for Na2. U_{ij} for Na1 have similar values regardless of x , in contrast to U_{ij} for Na2, which are anisotropic.

The atomic distances for the five $\text{Na}_x\text{Si}_{136}$ compositions are given in Table 3. The Si–Si bond lengths typically increase for $x > 8$ and remain relatively unchanged for $x < 8$. The average Si–Si bond lengths (Table 3) are 2.3548 Å for $\text{Na}_{2.9}\text{Si}_{136}$, 2.3540 Å for $\text{Na}_{5.1}\text{Si}_{136}$, 2.3551 Å for $\text{Na}_{8.2}\text{Si}_{136}$, 2.3595 Å for $\text{Na}_{14.7}\text{Si}_{136}$, and 2.3729 Å for $\text{Na}_{24}\text{Si}_{136}$. These are extended compared with the Si–Si bond lengths in $\alpha\text{-Si}$.⁵⁰ Upon filling the Si_{20} polyhedra, the average Na1–Si distances increase, in contrast to the nonmonotonic behavior of the average Na2–Si distances. The shortest Na1–Na1 distance for $\text{Na}_{8.2}\text{Si}_{136}$ is 5.1759 Å; however this distance is 5.2015 Å for $\text{Na}_{24}\text{Si}_{136}$. The shortest Na2–Na2 distances also increase with increasing x but not as strongly as the Na1–Na1 distances. The Na2–Na2 atomic distances have values ranging from 5.85 Å for $\text{Na}_{2.9}\text{Si}_{136}$ to 6.01 Å for $\text{Na}_{24}\text{Si}_{136}$.

An investigation into the transport properties of $\text{Na}_x\text{Si}_{136}$ clathrates is challenging due to the difficulty in obtaining highly

dense polycrystalline specimens. Because oxide readily forms on the surface of microcrystalline powders, densification of $\text{Na}_x\text{Si}_{136}$ powders has been very difficult.⁴⁶ In addition, this oxide formation screens the intrinsic transport properties measured on densified polycrystalline specimens.^{29,51} The synthesis technique described in the previous section allowed for the availability of dense homogeneous polycrystalline $\text{Na}_x\text{Si}_{136}$ in the form of agglomerations of single crystals.

The temperature dependence of the electrical and thermal properties with Na content was measured directly on these polycrystalline specimens. Figure 3 shows the temperature

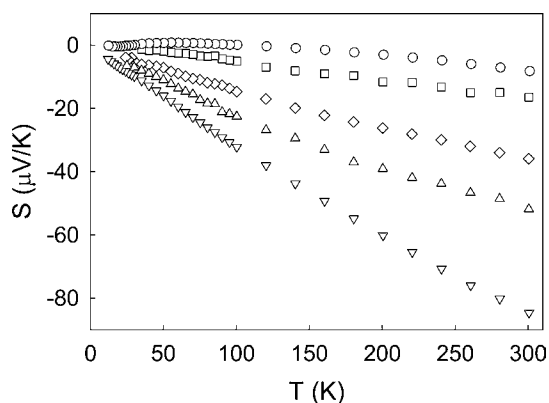


Figure 3. Seebeck coefficient as a function of temperature for $\text{Na}_x\text{Si}_{136}$ with $x = 2.9$ (∇), 5.1 (Δ), 8.2 (\diamond), 14.7 (\square), and 24 (\circ).

dependence of S for $\text{Na}_x\text{Si}_{136}$. The modulus of S increases with temperature, as expected in metals and heavily doped semiconductors with negligible phonon drag. The relatively low magnitude of S for $\text{Na}_{24}\text{Si}_{136}$ is typical for metals where the location of the Fermi level is well inside the conduction band, as indicated by density-functional theory calculations.^{26,52} As the Na content decreases, the modulus of S increases, reaching a value of $85 \mu\text{V/K}$ at room temperature for $\text{Na}_{2.9}\text{Si}_{136}$. According to theoretical studies by Smelyanski et al.,⁵² the similarity between the density of states profiles for Na (both 3s and 3p) and the total density of states indicates a significant hybridization between metallic Na and the Si framework wave functions when Si_{20} are filled. This is consistent with the metallic behavior of $\text{Na}_x\text{Si}_{136}$ for high Na loading. The average Na1–Si and Na2–Si distances decrease as x decreases to 8.2 (Table 3). This may imply a significant hybridization between Na and Si corroborating the metallic behavior for $x > 8$. For $x < 8$ however, there are no Na1, which presumably would reduce hybridization.

The temperature dependence of ρ indicates an apparent metal-to-semiconductor transition (Figure 4). There is a clear difference in the magnitude and temperature dependence of ρ as x changes from 2.9 to 24. The ρ values increase with increasing temperature for $x = 8.2$, 14.7 , and 24 , typical for metals, and decrease with increasing temperature for $x = 2.9$ and 5.1 , typical for semimetallic or semiconducting materials. The room temperature ρ value for $\text{Na}_{2.9}\text{Si}_{136}$ is over 2 orders of magnitude higher than that for $\text{Na}_{14.7}\text{Si}_{136}$ and 5 orders of magnitude lower than that of the lowest Na content $\text{Na}_x\text{Si}_{136}$ specimens hot pressed from powders.^{13,29} From quantum molecular dynamics studies on Si_{136} and $\text{Na}_4\text{Si}_{136}$, it was shown that Na moves away from the center of Si_{28} by 0.17 \AA .⁵³ From EXAFS studies on $\text{Na}_8\text{Si}_{136}$,⁴⁷ a strong interaction between Na2 results in Jahn–Teller distortion and Na_2 dimer formation,

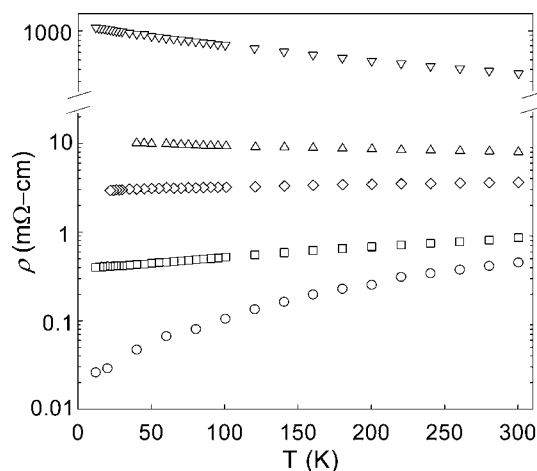


Figure 4. Resistivity (log scale) as a function of temperature for $\text{Na}_x\text{Si}_{136}$ with $x = 2.9$ (∇), 5.1 (Δ), 8.2 (\diamond), 14.7 (\square), and 24 (\circ).

possibly originating from the spin–spin interactions from the unpaired 3s electrons of Na. Our results show that the Na2–Na2 distances decrease as x decreases. The shortest Na2–Na2 distance for $\text{Na}_{24}\text{Si}_{136}$ is 6.01 \AA and decreases to 5.85 \AA for $\text{Na}_{2.9}\text{Si}_{136}$. Therefore partial covalent bonding between Na2 is more likely to occur at low Na concentrations. This partial covalent bonding between Na2,^{47,52,53} combined with the weak Na2–Si hybridization that results from the larger Na2–Si distances for $x < 8$ (Table 3), may result in localization of the electrons and “drive” the system to a less metallic state. Similar behavior in the endohedral metallofullerene $\text{Y}@C_{82}$ has been reported by Hasegawa et al.⁵⁴ Our experimental results corroborate prior theoretical work. Semiconducting behavior for $\text{Na}_4\text{Si}_{136}$ was predicted by the first principle full-potential all electron linearized plane wave method.⁵² It was suggested that the Jahn–Teller effect lifts the degeneracy at the Γ point and opens a small band gap.⁵² In addition, Mott⁵⁵ argued that the Na wave function overlap decreases as the Na concentration decreases, and the electrons become localized on the Na atoms. When this localization occurs, a Mott transition takes place and the system becomes semiconducting.⁵⁵ This is corroborated by the increase in the Na–Si distances for $x < 8$. As Na moves away from the Si framework atoms, there may be less hybridization between Na and Si, which results in localization of the electrons around Na. The shortest Na–Na distance (5.1759 \AA) excludes the possibility of direct Na–Na interaction, as also suggested by Roy et al.⁴⁹

The thermal conductivities for the five $\text{Na}_x\text{Si}_{136}$ specimens are shown in Figure 5. The magnitude of κ is relatively large compared with that of other intermetallic clathrates.⁶ The observed κ for $\text{Na}_{24}\text{Si}_{136}$ is higher than the other clathrates shown in Figure 5 because it is dominated by the electronic component.³⁶ The room temperature values of κ for $\text{Na}_{2.9}\text{Si}_{136}$ and $\text{Na}_{5.1}\text{Si}_{136}$, the two specimens with the lowest Na content, are approximately three times lower than that of $\text{Na}_{24}\text{Si}_{136}$.

4. CONCLUSION

Single crystals of $\text{Na}_{2.9}\text{Si}_{136}$, $\text{Na}_{5.1}\text{Si}_{136}$, $\text{Na}_{8.2}\text{Si}_{136}$, and $\text{Na}_{14.7}\text{Si}_{136}$ were synthesized for the first time by thermal decomposition of $\text{Na}_{24}\text{Si}_{136}$ single crystals at $405 \text{ }^\circ\text{C}$. The Na content was controlled by the duration of the thermal decomposition. Structural properties as a function of Na were characterized by single-crystal X-ray diffraction. The high-density polycrystalline

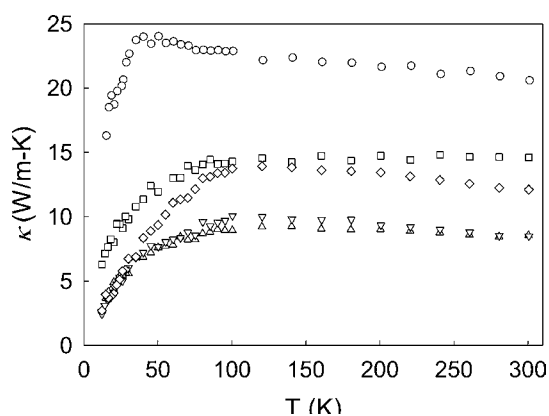


Figure 5. Thermal conductivity as a function of temperature for $\text{Na}_x\text{Si}_{136}$ with $x = 2.9$ (∇), 5.1 (Δ), 8.2 (\diamond), 14.7 (\square), and 24 (\circ).

$\text{Na}_x\text{Si}_{136}$ specimens resulting from our synthesis technique allowed for an investigation of the low-temperature transport properties as a function of Na content. The $\text{Na}_{2.9}\text{Si}_{136}$ and $\text{Na}_{5.1}\text{Si}_{136}$ specimens indicate nonmetallic behavior, in corroboration with the expected metal-to-insulator transition at $x \approx 8$.^{52,55}

■ ASSOCIATED CONTENT

📄 Supporting Information

Crystallographic data in CIF format for the single crystal $\text{Na}_x\text{Si}_{136}$ specimens. This material is available free of charge via the Internet at <http://pubs.acs.org>.

■ AUTHOR INFORMATION

Corresponding Author

*E-mail: gnolas@usf.edu.

Notes

The authors declare no competing financial interest.

■ ACKNOWLEDGMENTS

S.S. and G.S.N. acknowledge support by the U.S. Department of Energy, Basic Energy Sciences, Division of Materials Science and Engineering, under Award No. DE-FG02-04ER46145 for single crystal structural analyses, measured and simulated pXRD, SEM and low temperature transport measurements. At Northwestern University, single-crystal XRD was supported as part of the Revolutionary Materials for Solid State Energy Conversion, an Energy Frontier Research Center funded by the U.S. Department of Energy, Office of Science, Office of Basic Energy Sciences under Award Number DE-SC0001054.

■ REFERENCES

- (1) Nolas, G. S.; Slack, G. A.; Schujman, S. B. In *Semiconductors and Semimetals*; Tritt, T. M., Ed.; Academic Press: San Diego, CA, 2000; Vol. 69, p 255.
- (2) Adams, G. B.; O'Keefe, M.; Demkov, A. A.; Sankey, O. F.; Huang, Y.-M. *Phys. Rev. B* **1994**, *49*, 8048.
- (3) Moriguchi, K.; Munetoh, S.; Shintani, A. *Phys. Rev. B* **2000**, *62*, 7138.
- (4) Connetable, D. *Phys. Rev. B* **2007**, *75*, No. 125202.
- (5) Nolas, G. S.; Cohn, J. L.; Slack, G. A.; Schujman, S. B. *Appl. Phys. Lett.* **1998**, *73*, 178.
- (6) Cohn, J. L.; Nolas, G. S.; Fessatidis, V.; Metcalf, T. H.; Slack, G. A. *Phys. Rev. Lett.* **1999**, *82*, 779.

- (7) Hermann, R. P.; Keppens, V.; Bonville, P.; Nolas, G. S.; Grandjean, F.; Long, G. J.; Christen, H. M.; Chakoumakos, B. C.; Sales, B. C.; Mandrus, D. *Phys. Rev. Lett.* **2006**, *97*, No. 017401.
- (8) Phan, M. H.; Woods, G. T.; Chaturvedi, A.; Stefanoski, S.; Nolas, G. S.; Srikanth, H. *Appl. Phys. Lett.* **2008**, *93*, No. 252505.
- (9) Kawaji, H.; Horie, H. O.; Yamanaka, S.; Ishikawa, M. *Phys. Rev. Lett.* **1995**, *74*, 1427.
- (10) Yamanaka, S.; Enishi, E.; Fukuoka, H.; Yasukawa, M. *Inorg. Chem.* **2000**, *39*, 56.
- (11) Ramachandran, G. K.; Dong, J. J.; Diefenbacher, J.; Gryko, J.; Marzke, R. F.; Sankey, O. F.; McMillan, P. F. *J. Solid State Chem.* **1999**, *145*, 716.
- (12) Reny, E.; Gravereau, P.; Cros, C.; Pouchard, M. *J. Mater. Chem.* **1998**, *8*, 2839.
- (13) Cros, C.; Pouchard, M.; Hagenmuller, P. *J. Solid State Chem.* **1970**, *2*, 570.
- (14) Beekman, M.; Nolas, G. S. *J. Mater. Chem.* **2008**, *18*, 842.
- (15) Bobev, S.; Sevov, S. C. *J. Am. Chem. Soc.* **1999**, *121*, 3796.
- (16) San-Miguel, A.; Kéghélian, P.; Blase, X.; Mélinon, P.; Perez, A.; Itié, J. P.; Polian, A.; Reny, E.; Cros, C.; Pouchard, M. *Phys. Rev. Lett.* **1990**, *83*, 5290.
- (17) Ramachandran, G. K.; McMillan, P. F.; Deb, S. K.; Somayazulu, M.; Gryko, J.; Dong, J. J.; Sankey, O. F. *J. Phys.: Condens. Matter* **2000**, *12*, 4013.
- (18) McMillan, P. F. *Nat. Mater.* **2000**, *1*, 19.
- (19) San-Miguel, A. *Chem. Soc. Rev.* **2006**, *35*, 876.
- (20) Toulemonde, P.; San-Miguel, A.; Merlen, A.; Viennois, R.; Le Floch, S.; Adessi, Ch.; Blasé, X.; Tholence, J. L. *J. Phys. Chem. Solids* **2006**, *67*, 1117.
- (21) Cros, C.; Pouchard, M.; Hagenmuller, P. *C. R. Hebd. Seances Acad. Sci.* **1965**, *260*, 4764.
- (22) Kasper, J. S.; Hagenmuller, P.; Pouchard, M.; Cros, C. *Science* **1965**, *150*, 1713.
- (23) Cros, C.; Pouchard, M.; Hagenmuller, P.; Kasper, J. S. *Bull. Soc. Chim. Fr.* **1968**, 2737.
- (24) Nolas, G. S.; Slack, G. A. *Am. Sci.* **2001**, *89*, 136.
- (25) Slack, G. A. *Mater. Res. Soc. Symp. Proc.* **1997**, *478*, 47.
- (26) Conesa, J. C.; Tablero, C.; Wahn, P. *J. Chem. Phys.* **2004**, *120*, 6142.
- (27) Stefanoski, S.; Beekman, M.; Wong-Ng, W.; Zavalij, P.; Nolas, G. S. *Chem. Mater.* **2011**, *23*, 1491.
- (28) Beekman, M.; Nenghabi, E. N.; Biswas, K.; Myles, C. W.; Baitinger, M.; Grin, Y.; Nolas, G. S. *Inorg. Chem.* **2010**, *49*, 5338.
- (29) Beekman, M.; Nolas, G. S. *Physica B* **2006**, *383*, 111.
- (30) Beekman, M.; Baitinger, M.; Borrmann, H.; Schnelle, W.; Meier, K.; Nolas, G. S.; Grin, Yu. *J. Am. Chem. Soc.* **2009**, *131*, 9642.
- (31) Gryko, J.; Marzke, R. F.; Lambertson, G. A., Jr.; Tritt, T. M.; Beekman, M.; Nolas, G. S. *Phys. Rev. B* **2005**, *71*, No. 115208.
- (32) Guloy, A. M.; Ramlau, R.; Tang, Z.; Schnelle, W.; Baitinger, M.; Grin, Yu. *Nature* **2006**, *443*, 320.
- (33) Simon, P.; Tang, Z.; Carrillo-Cabrera, W.; Chiong, K.; Böhme, B.; Baitinger, M.; Lichte, H.; Grin, Yu.; Guloy, A. M. *J. Am. Chem. Soc.* **2011**, *133*, 7596.
- (34) Stefanoski, S.; Martin, J.; Nolas, G. S. *J. Phys.: Condens. Matter* **2010**, *22*, 485404.
- (35) Nolas, G. S.; Vanderveer, D. G.; Wilkinson, A. P.; Cohn, J. L. *J. Appl. Phys.* **2002**, *91*, 8970.
- (36) Beekman, M.; Schnelle, W.; Borrmann, H.; Baitinger, M.; Grin, Yu.; Nolas, G. S. *Phys. Rev. Lett.* **2010**, *104*, No. 018301.
- (37) Beekman, M.; Hermann, R. P.; Möchel, A.; Juranyi, F.; Nolas, G. S. *J. Phys.: Condens. Matter* **2010**, *22*, No. 355401.
- (38) Nolas, G. S.; Ward, J. M.; Gryko, J.; Qiu, L.; White, M. A. *Phys. Rev. B* **2001**, *64*, No. 153201.
- (39) Rogl, P. In *Thermoelectrics Handbook: Macro to Nano*; Rowe, D. M., Ed.; CRC Press: Boca Raton, FL, 2006; p 32-1.
- (40) Beekman, M.; Kaduk, J. A.; Gryko, J.; Wong-Ng, W.; Shapiro, A.; Nolas, G. S. *J. Alloys Comp.* **2009**, *470*, 365.
- (41) Mansour, A. N.; Beekman, M.; Wong-Ng, W.; Nolas, G. S. *J. Solid State Chem.* **2009**, *182*, 107.

- (42) Martin, J.; Nolas, G. S.; Wang, H.; Yang, J. *J. Appl. Phys.* **2007**, *102*, No. 103719.
- (43) Horie, H.; Kikudome, T.; Teramura, K.; Yamanaka, S. *J. Solid State Chem.* **2009**, *182*, 129.
- (44) Sloan, E. D. *Clathrate Hydrates of Natural Gases*; Marcel Dekker Inc.: New York, 1998.
- (45) Ritchie, A.; MacDonald, M.; Zhang, P.; White, M. A.; Beekman, M.; Gryko, J.; Nolas, G. S. *Phys. Rev. B* **2010**, *82*, No. 155207.
- (46) Beekman, M.; Sebastian, C. P.; Grin, Yu.; Nolas, G. S. *J. Electron. Mater.* **2009**, *38*, 1136.
- (47) Brunet, F.; Mélinon, P.; San Miguel, A.; Kéghélian, P.; Perez, A.; Flank, A. M.; Reny, E.; Cros, C.; Pouchard, M. *Phys. Rev. B* **2000**, *61*, 16550.
- (48) Stefanoski, S.; Nolas, G. S. *Cryst. Growth Des.* **2011**, *11*, 4533.
- (49) Roy, S. B.; Sim, K. E.; Caplin, D. *Philos. Mag. B* **1992**, *65*, 1445.
- (50) Goryunova, N. A. *The Chemistry of Diamond-like Semiconductors*; MIT Press: Cambridge, MA, 1963.
- (51) He, J.; Klug, D. D.; Uehra, K.; Preston, K. F.; Ratcliffe, C. I.; Tse, J. S. *J. Phys. Chem. B* **2001**, *105*, 3475.
- (52) Smelyanski, V. I.; Tse, J. S. *Chem. Phys. Lett.* **1997**, *264*, 459.
- (53) Demkov, A.; Sankey, O. F.; Schmidt, K. E.; Adams, G. B.; O'Keeffe, M. *Phys. Rev. B* **1994**, *50*, 17001.
- (54) Hasegawa, Y.; Ling, Y.; Yamazaki, S.; Hashizume, T.; Shinohara, H.; Sakai, A.; Pickering, H. W.; Sakurai, T. *Phys. Rev. B* **1997**, *56*, 6470.
- (55) Mott, N. F. *J. Solid State Chem.* **1973**, *6*, 348.